Quantum Mechanical Study of the O(¹D) + HCl → OH + Cl Reaction

Shi Ying Lin and Seung C. Park*

Department of Chemistry and Institute of Basic Sciences, Sungkyunkwan University, Suwon 440-746, Korea
Received January 3, 2002

Quantum mechanical calculation is performed for the O(¹D) + HCl → OH + Cl reaction using Reactive Infinite Order Sudden Approximation. Shifting approximation is also employed for the $l \neq 0$ partial wave contributions. Various dynamical quantities are calculated and compared with available experimental results and quasiclassical trajectory results. Vibrational distributions agree well with experimental results *i.e.* product states mostly populated at v_f = 3, 4. Our results also show small peak at v_f = 0, which indicates bimodal vibrational distribution. The results show two significant broad peaks in γ_i dependence of the cross section, one is at γ_i = 15°-35° and the another is at γ_i = 55°-75° which can be explained as steric effects. At smaller γ_i, the distribution is peaked only at higher state (v_f = 3, 4) while at the larger γ_i, both lower state (v_f = 0) and higher state (v_f = 3, 4) are significantly populated. Such two competing contributions (smaller and larger γ_i) result in the bimodal distribution. From these points we suggest two mechanisms underlying in current reaction system: one is that reaction occurs in a direct way, while the another is that reaction occurs in a indirect way.

Keywords : RIOS, O(¹D), Vibrational state distributions, Rate constants.

Introduction

One of the important function of the ozone layer located in the stratosphere is that it shields earth from harmful solar UV radiation.[1] Various chemical reactions are undergoing in this layer and the quantity of the ozone is preserving constant naturally through the auto-balanced production and depletion.[1] Therefore the ozone related research is of great importance.

O(¹D) produced by photolysis from O_3 initiates many important reactions, it reacts easily with many chemically stable substances in stratosphere and their products catalytically destroy O_3 layer.[1] HCl, its chemical and photochemical stability makes it an ideal sink for the chemically active chlorine, reacts with O(¹D) very quickly and its products form catalytic cycle for the consumption of O_3 layer.[2] Such significant affect on O_3 layer, stimulated extensive experimental works since the early years.[2-13]

O(¹D) is deactivated by HCl *via* three competing pathways:[3]

$$O(^1D) + HCl \rightarrow OH + Cl,\ \Delta H = -44\ \text{kcal/mol} \quad (1a)$$

$$O(^1D) + HCl \rightarrow H + ClO,\ \Delta H = -6\ \text{kcal/mol} \quad (1b)$$

$$O(^1D) + HCl \rightarrow O(^3P) + HCl,\ \Delta H = -45\ \text{kcal/mol} \quad (1c)$$

Davidson *et al.*[4] first measured the total rate constant for the deactivation of O(¹D) by HCl at 298 K. ($1.4(\pm 40\text{-}50\%) \times 10^{-10}$ cm³/molecule/sec). In subsequent work[5] the temperature dependence of the rate constants was measured with more accuracy, and the authors found the rate constant is nearly constant ($1.3\text{-}1.5(\pm 30\%) \times 10^{-10}$ m³/molecule/sec) over the temperature range (199-379 K). Arrhenius activation energies are calculated to be negligibly small (less than 20 cal/mol). They also have come to conclusion that the channel (1b) is minor reaction path.

Addison *et al.*[6] performed an experiment aiming to determine the relative importance between channel (1a) and (1b). They pointed out that the ClO which was observed in the earliest experiment[7] for the current reaction system is produced through another reaction rather than through the reaction (1), and they further concluded the channel (1a) is the only primary channel. Much later Wine *et al.*[3] have given the quantitative branching ratio between the three competing pathways of reaction (1) at 297 K. Their results show that while the channel (1a) is predominant pathway (67 ± 10%), the other two channels are not negligible (24 ± 5 for (1b), 95 % for (1c)), especially the channel (1b) significantly contribute to the reaction (1). They also determined the overall rate of reaction (1) ($1.50 \pm 0.3 \times 10^{-10}$ cm³/molecule/sec) which is in good agreement with that of Davidson *et al.*[4,5] Recently energy specific branching ratios also have been reported.[8,9] Balucani *et al.*[8] have given the lower limit of the branching ratio $\sigma(ClO)/\sigma(OH) \geq 0.34 \pm 0.10$ at collision energy of 12.2 kcal/mol, and Matsumi *et al.*[9] obtained 0.24 ± 0.06 at 7.6 kcal/mol. Both of them are in good accord with the previous result ($k(OCl)/k(OH) = 0.36 \pm 0.10$ at 297 K).[3] They also have found strong isotope effect on the channel branching ratio in their experiment substituting the hydrogen H to its isotope D in the reaction (1) ($\sigma(ClO)/\sigma(OD) \geq 0.09 \pm 0.02$ at 7.7 kcal/mol).

Parallel with these experiments related to the branching ratio or rate constant measurements, experiments[2,7,8,10-12] related to the various product distribution-PRD (Product Rotational Distribution), PVD (Product Vibrational Distribution)[2,7,10,11] and PAD (Product Angular Distribution)[8,12] are also carried out extensively. Except on experiment[8] which exceptionally studied only for the channel (1b), all the other

*To whom correspondence should be addressed. e-mail: scpark @chem.skku.ac.kr

studies are concerned with the channel (1a). These kinds of experiments are more helpful for getting insight into the dynamics of the reaction. These experiments really have provided abundant dynamical information, and the reaction mechanism was extensively discussed by the authors. Basco *et al.*[8] first demonstrated qualitatively in their flash photolysis-kinetic absorption experiment that OH is produced with considerable vibrational excitation. Much later Luntz[10] measured the OH internal state distribution. They reported highly inverted rotational distribution for OH (v'=0) and OH (v'=1) and also reported the vibrational population ratio P(v'=1)/P(v'=0)=1.5. Kruus *et al.*[2] have obtained highly inverted OH vibrational distribution, v'=3, 4 are found to be the maximally populated levels while v'=1 and v'=2 levels are nearly not populated. The population for v'=0 can not be measured with their experimental method. They also have obtained very small vibrational distribution of HCl which produced through the channel (1c). Park *et al.*[11] also have obtained excited ro-vibrational distributions. Their rotational states are inverted almost up to the exothermicity and vibrational states are also highly excited, peaking at v'=4, agree quite well with the PVD of Kruus *et al.*[2] Balucani *et al.*[8] have given the PAD for the ClO product of the reaction (1b), and very recently Alexander *et al.*[12] have measured the PAD of OH (v'=4, N=6) product of the reaction (1a). Although the two PADs are for two different channels, their features are similar *i.e.* almost backward-forward symmetric, with backward scattering being favored. They found that the PAD is shifting from the backward towards the forward hemisphere while the energy is increased. They have also measured the energy dependent relative cross sections. The cross sections are shown to be monotonically decreasing with the energy.

Most of the authors of those experiments[9-12] suggested the dominance of the insertion type of reaction mechanism for the reaction channel (1a) from various points of view, *i.e.* O(^{1}D) first inserts into HCl (*via* ground ^{1}A' surface) to form highly excited HOCl complex. This complex then subsequently breaks into the product pieces. The recent stereodynamic study[12] also emphasized the role played by the abstraction mechanism while they still agree on the dominant role played by the insertion reaction. In spite of the formation of the complex, the product have shown the non-statistical highly inverted internal state distributions. This contribution is explained by those authors that the lifetime of the complex is not long enough so that the complex fragments before energy is equipartitioned. Concerning with the channel (1b) Matsumi *et al.*[9] suggested from the isotope effects that the reaction is dominated by the abstractions, while Balucani *et al.*[8] suggested from the PAD that although significant part of reaction is due to the abstraction, the contribution from insertion type of reaction can not be ruled out.

When experiments are done, it is alway desirable that theoretical study explain the measured results reasonably. Schinke[14] has performed quasi-classical (QC) calculation on the adiabatic potential energy surface (PES) which is fitted from the *ab initio* data.[15] This study reproduced Luntz's[10] experimental results very nicely, while the PVD shows less excitation in contrast to the later experiments.[2-11] On account of the inaccurate potential feature for the channel (1b) the branching ratio σ(ClO)/σ(OH) is too much underestimated. In contrast to the recent measured PAD[12] which displays favoring in backward scattering, Schinke's result shows slight preference for forward scattering. Schinke finally has come to the conclusion that the reaction is predominantly insertion type and abstraction is negligible. Rynefors *et al.*[16] have successfully simulated non-statistical experimental rotational distributions[10] using their statistical algorithm, but failed to simulate the vibrational distributions. Very recently two more QC studies[17,18] have done using new PESs. Lagan *et al.*[17] have set up PES which has the correction asymptotic limits for both channels of (1a) and (1b) from the limited information.[19-23] Their QC calculation on this PES has obtained reasonable branching ratios and PAD. The rate constants are several times smaller than the experimental results and PAD is poor agreement with experiments, poorer than the previous QC study.[14] Hernadez *et al.*[18] have calculate a new *ab initio* PES and fitted to analytic form. QC calculation have done on this PES and successfully well all the available experimental results except for the PVD.

So far, there is no quantum mechanical study performed for current reaction system, in spite of the fact that in this reaction system, the quantum mechanical effects may play essential role, because it is a light atom transfer reaction and the PES possesses a deep potential well. There are several reasons that prohibit the quantum mechanical study for this system. One is that the larger exothermicity and deep potential well of current reaction system opens numerous ro-vibration channels which is one of the main factor that burden the calculation. Another one is that this reaction is a heavy atom reaction and the potential has long range part, and for such reaction one has to calculate many partial wave contribution in order to get converged cross sections. Another very difficult problem is that the current reaction system is not a collinear dominated system, and for such system, it is hard to apply approximate quantum theories. Quantum mechanical description for such reaction is major unsolved problem in chemical dynamics.[24]

Reactive Infinite Order Sudden Approximation (RIOSA)[25-71] is one of the most important and widely used approximation theory in reactive collisions with very economic computation. Since this theory proposed by several group.[25-29] it has been successfully applied to various atom-diatom reaction system.[25-44] In this work we have employed RIOS to study the current reaction system quantum mechanically using Schinke's PES.[14] The applicability of RIOS to such non-collinear reaction is not clear, therefore current study might give some answer about the validity of the RIOSA for such an non-collinear HLH reaction system.

Theory

Several versions exist within the RIOSA theory,[35] among them the *l*-initial (*l*-in)version is the simplest one. In the *l*-in

RIOSA, the state to state cross section for A + BC(v_i, j_i) AB(v_f, all j_f) + C reaction is simply given by[28,32,35,36,43]

$$\sigma(j_i, v_i \rightarrow v_f; E_{tr}) = \frac{\pi}{2k^2_{v_i j_i}} \sum_{l_i} (2l_i + 1) \int_0^{\pi} d\gamma_i \sin\gamma_i \, P_{l_i}(j_i, v_i \rightarrow v_f, \gamma_i, E_{tr}) \quad (2)$$

where

$$P_{l_i}(j_i, v_i \rightarrow v_f, \gamma_i, E_{tr}) = \left| S_{l_i}(j_i, v_i \rightarrow v_f, \gamma_i, E_{tr}) \right|^2 \quad (3)$$

is the reaction probability for l_i partial wave, and S_{l_i} $(j_i, v_i \rightarrow v_f, \gamma_i, E_{tr})$ is the corresponding scattering, γ_i is the angles as shown in Figure 1, $k_{v_i j_i}$ is the wave number of incoming channel and $E_{tr} = \hbar^2 k^2_{v_i j_i} / 2\mu_{A,BC}$ ($\mu_{A,BC}$ is the reduced mass of atom A and molecule BC) is the initial relative translational energy. In order to obtain the scattering matrix, the following collinear-like partial differential equation[43] should be solved numerically in each channel

$$\left[-\frac{\hbar^2}{2\mu} \left(\frac{\partial^2}{\partial R_\lambda^2} + \frac{\partial^2}{\partial r_\lambda^2} \right) + \frac{l_{\lambda}(l_{\lambda}+1)}{2\mu R_\lambda^2} + V(R_\lambda, r_\lambda, \gamma_\lambda) \right] x(R_\lambda, r_\lambda, \gamma_\lambda) = E x(R_\lambda, r_\lambda, \gamma_\lambda) \quad (4)$$

where λ (= i, f) denotes the reaction channel and μ, R_λ, r_λ is defined by

$$\mu = \left(\frac{m_A m_B m_C}{m_A + m_B + m_C} \right)^{\frac{1}{2}} \quad (5a)$$

$$R_\lambda = b_\lambda \overline{R}_\lambda \qquad r_\lambda = b_\lambda^{-1} \overline{r}_\lambda \quad (5b)$$

$$b_i = \left(\frac{\mu}{\mu_{BC}} \right)^{\frac{1}{2}} \qquad b_f = \left(\frac{\mu}{\mu_{AB}} \right)^{\frac{1}{2}} \quad (5c)$$

where $\overline{R}_\lambda$, $\overline{r}_\lambda$ are the atom-diatom distance and diatom distance for λ (= i, f) channel as depicted in Figure 1. μ_{BC}, μ_{AB} are the reduced masses of AB,BC diatoms respectively. γ_λ ($\lambda = i, f$) are the angles as depicted in Figure 1, (and) they enter into eq. (4) as parameters rather than as variables by RIOSA assumption *i.e.* both angles are fixed in each channels. (γ_i is fixed for reactant and γ_f is fixed for product channel) With such RIOSA assumption, the whole configuration space of the reaction system is separated into two parts -the γ_i fixed part and the γ_f fixed part, then one problem arises as to how and where to match the two parts of configuration spaces. Generally there exist two kinds of method of matching discussed so far. In one method, the two angles (γ_i and γ_f) are completely independent and for any pair of γ_i and γ_f, the matching line is naturally defined correspondingly. this is called two-angle dependent RIOSA.[35,37,39,40,42] In another method, two angles are one-to-one correlated *i.e.* for any chosen γ_i, γ_f is uniquely defined. In this case a matching line should be imposed artificially. The first method is computationally much more expensive than the second one. therefore it is seldom used in practical quantum mechanical RIOSA calculation. The second method is the mostly used one in practical applications. Our current work also employed the second method.

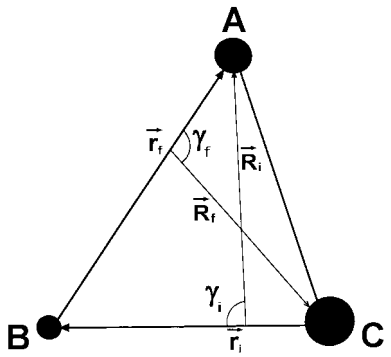

Figure 1. Jocobian coordinates of A + BC system.

In case of two angles correlated one-to-one, additional matching line should be imposed. This line is usually defined as

$$r_f = B_{fi} r_i \quad (6)$$

where the B_{fi} is the matching coefficient. The matching in RIOSA theory is intrinsically different from the accurate theory where the matching does not affect the final results in principle. It does only affect the efficiency of the calculation. In case of RIOSA the different matching results in different effective hamiltonian, and subsequently affects the final results directly. Therefore the matching coefficient B_{fi} should be chosen carefully. For the symmetric reaction system like H + H_2 reaction B_{fi} could be reasonably taken to be 1. But in case of general non-symmetric reaction systems, there has not yet convincing theoretical guide for the unambiguous determination of the matching coefficient B_{fi}. Nakamura *et al.*[43] have proposed a reasonable method of determining the B_{fi}. The values of B_{fi} varying with γ_i taking attention to the important role of potential ridge in reaction. With the matching equation defined by eq. (6), γ_f is determined uniquely by

$$\cos\gamma_f = -\frac{\cos\gamma_i - (1 - B_{fi}^2)\tan\alpha_i \cot\beta_{fi}}{B_{fi}[1 + (1 - B_{fi}^2)\tan^2\alpha_i]^{1/2}} \quad (7)$$

where β_{fi} is the collinear skew angle, and α_i is the matching angle from the axis of R_i in the R_i-R_f skewed coordinate *i.e.* the angle between R_i axis and matching line. they are given by[25,35,36,42,43]

$$\beta_{fi} = \tan^{-1}(m_B/\mu) \quad (8)$$

$$\tan\alpha_i = \frac{\sin\beta_{fi}[-\cos\beta_{fi}\cos\gamma_i + (B_{fi}^2 - \sin^2\gamma_i\cos^2\beta_{fi})^{1/2}]}{\beta_{fi} - \cos^2\beta_{fi}} \quad (9)$$

Similarly, α_f is the matching angle from the axis of R_f, and is given by

$$\tan\alpha_f = \frac{B_{fi}\tan\alpha_i}{[1 + (1 - B_{fi}^2)\tan^2\alpha_i]^{1/2}} \quad (10)$$

Then the non-collinear skew angle is given by[43]

$$\beta_{fi}(\gamma_i) = (\alpha_i + \alpha_f) \tag{11}$$

Now the only parameter to be determined is the l_f, and this can be naturally determined by the requirement of continuity of the hamiltonian,[29,41] so the centrifugal potential should be conserved along the matching line[29,41,43] *i.e.*

$$\frac{l_i(l_i+1)}{R_i^2} = \frac{l_f(l_f+1)}{R_f^2} \tag{12}$$

and using the following equality at the matching line[43]

$$\frac{R_f}{R_i} = \frac{r_f(r_i/R_i)}{r_i(r_f/R_f)} = B_{fi}\frac{\tan\alpha_i}{\tan\alpha_f} \tag{13}$$

the l_f is then determined.

Although RIOSA greatly reduced the computer time, large amount of computation is still needed usually, especially for heavy atom reaction systems in order to get the converged cross sections. One has to calculate hundreds of partial wave contributions, this means one must repeat hundreds of numerical calculations of partial differential equation (4), and such a calculation should be performed several times for several chosen γ_i angles. Shifting approximation[45,46] (or CCPA[44,47]) is quite useful in such a case. With this approximation only $l = 0$ partial wave calculation is needed. The contributions of $l \neq 0$ partial waves are approximated from $l = 0$ as[44,47]

$$P_{l_i}(j_i,v_i \rightarrow v_f;\gamma_i,E_{tr}) \approx P_{l=0}(j_i,v_i \rightarrow v_f;\gamma_i,E_{tr}-B^{\dagger}l_i(l_i+1)) \tag{14}$$

where

$$B^{\dagger} = B^{\dagger}(\gamma_i) = \frac{\hbar^2}{2\mu R^{\dagger 2}} \tag{15}$$

$R^{\dagger} = R^{\dagger}(\gamma_i)$ is a representative value which are usually chosen to be at transition state[45,46] or on potential ridge line.[44,47] Additionally using the following approximate equality[44-47]

$$\sum_{l_i}(2l_i+1)P_{l_i}(j_i,v_i \rightarrow v_f;\gamma_i,E_{tr}) \approx \frac{1}{B^{\dagger}(\gamma_i)} \int_0^{E_{tr}} d\varepsilon P_{l=0}(j_i,v_i \rightarrow v_f;\gamma_i,\varepsilon) \tag{16}$$

Cross section given in eq. (2) could further be expressed as[44]

$$\sigma(j_i,v_i \rightarrow v_f;E_{tr}) = \frac{\pi}{2k_{v_ij_i}^2}\int_0^{\pi} d\gamma_i \frac{\sin\gamma_i}{B^{\dagger}(\gamma_i)} \int_0^{E_{tr}} d\varepsilon P_{l_i=0}(j_i,v_i \rightarrow v_f;\gamma_i,\varepsilon) \tag{17}$$

Thus the shifting approximation transformed the work for the summation of many partial wave contribution into the work for the integration over the energy, only one partial wave contribution at several energies should be calculated. This save computer time greatly.

Once the cross sections at many energies are obtained, rate constants are also can be calculated using the equation[48]

$$k(j_i,v_i \rightarrow v_f;T) = \frac{1}{k_BT}\left(\frac{8}{\pi\mu_{A,BC}k_BT}\right)^{1/2} \int_0^{\infty} dEEe^{-E/k_BT}\sigma(j_i,v_i \rightarrow v_f;E) \tag{18}$$

where k_B is the Boltzmann constant and T is the temperature.

Numerical Method and Matching Coefficient

A. Numerical method. In order to obtain the state-to-state reaction probability and cross section in RIOSA we should solve the collinear-like two dimensional differential equation given by eq. (4). This can be done accurately using several numerical methods. *R*-matrix method[49-53] proved to be quite efficient and numerically stable. It is especially favourable when one needs to calculate reaction probability at many energies.

In case of reactive scattering, the efficiency of the numerical solution for the partial differential equation also largely depends upon the suitable choice of coordinate system. Since Kupperman[54] imposed hyperspherical coordinate into chemical reaction scattering calculations, it is widely used in various reaction system,[55] and it became one of the most advantageous coordinate. This coordinate system is not only numerically efficient but also very helpful for the analysis of reaction mechanism by plotting the vibrationally adiabatic potential (VAP)[47] curves as a function of hyperradius.

Nakamura *et al.*[43] have proposed to impose hypershperical coordinate to RIOSA, and such a method is employed here. In our numerical treatment, we employed the hyperspherical coordinate in the interaction region and it is transformed to Jacobian coordinate at near asymptotic region (large hyperradius). *R*-matrix method is also employed to obtain the scattering matrix.

R-matrix is propagated along the sectors which are divided along the hyperradius, starting from small enough hyperradius (where potential energy is high enough). In each sectors, local vibrational bound states (for the vibrational along the hyperangle with fixed hyperradius) obtained numerically by finite difference method are employed as the basis sets for the expansion of the wavefunction. Total 30 vibrational channels are included. This number is large enough to cover all the open channels for any chosen γ_i angles at least, and also includes quite number of closed channels. In order to check the convergence with respect to the channel number, we have compared the results of employed 30 vibrational channels with the results of employing less number of vibrational channels for several chosen γ_i angles, and we have found that the differences are not significant, especially the total reaction probability and cross sections. Vibrational distributions have only negligible changes.

The shifting position $R^{\dagger}$ is chosen to be on the matching line and such a ρ (hyperradius) where the potential along the

hyperangle (for fixed hyperradius) changes from double well to single well. as suggested by Park *et al.*[47] The integration over γ_i in eq. (2) is performed using the gaussian quadrature method. We have taken 10 gaussian quadrature points for the integration over [0. $\pi/2$] and the integration over [$\pi/2$, π] is neglected. The integration over the translational energy in eq. 917) is performed using simple extended trapezoidal method with step size $\Delta\varepsilon = 0.5$ kcal/mol.

B. Matching coefficient. As already mentioned in section 2, the matching coefficient, B_{fi} can not be taken arbitrarily. For a general nonsymmetric reaction systems. reasonable value of B_{fi} should be determined by carefully investigating the PES topography. Nakamura *et al.*[43] have proposed an iterational method of determining the B_{fi}. In this paper we introduced a new method to determine the γ_i dependent B_{fi}.

Making contour figure as a function of r_i and r_f for fixed γ_i we can reasonably determine the value of B_{fi}, at least the reasonable range of B_{fi} can be determined from such figure, within that range the final calculated results are expected to slightly depend on the value of B_{fi}.

Figure 2 is such kind of figure for $\gamma_i = 32.89°$. Because the γ_i is fixed. this figure does not represent full configuration space of the reaction system, but only represents half part (reactant and part of interaction) of the full configuration space, and another half part will be provided by the γ_f fixed configuration space. In making such figures one problem arises because for a fixed γ_i. the r_i and r_f do not always uniquely determine the three internuclear distances so the PES will not be uniquely defined. As shown in Figure 3. when $\bar{r}_f < x$ two different positions are possible for atom A (A and A') for a single pair of r_i, r_f value. We have taken only the outer position (A), because the inner position (A') will be

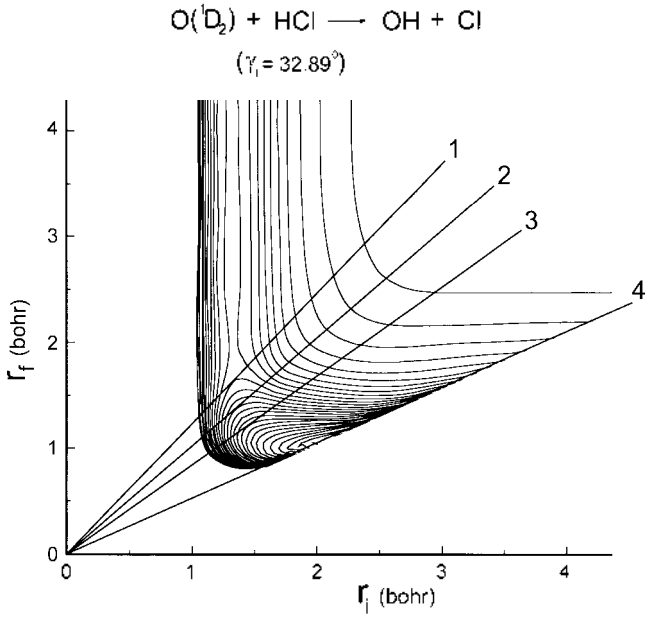

Figure 2. Potential contour of O(¹D) + HCl system as a function of reduce mass Jocobian coordinates- r_i and r_f with γ_i (γ_i = 32.89°) being fixed. The line labeled by 1, 2, 3, 4 are described in the text.

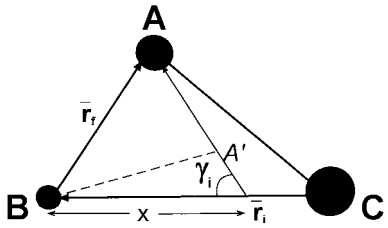

Figure 3. Jocobian coordinates of A + BC system. It is given in order to illustrate the problem during making coutour figures like Figure 2.

very close to the atom C (because of heavy mass of atom C).

In this countour figure a line passing through the origin will determine the matching line in RIOSA theory, the slope of this line will be the matching coefficient B_{fi}. In Figure 2, four lines are drawn, line-4 representing the minimum limitation of the matching line, its slope is given by $B_{fi(min)} = \sin\gamma_i \cos\beta_{fi}$,[35] B_{fi} can not be smaller than this value.

Observing the PES topography, we could find in the upper part of line-1. PES shows reactant-like shape and when goes down PES topography changes significantly and after line-3 PES begin to show product-like topography. Therefore it's reasonable to consider that the switching between two channels occurred in the region between line-1 and line-3. Among the lines between line-1 and line-3 the line-2 follows well the potential ridge. so we have chosen line-2 as the matching line in our calculation. Its slope can be obtained directly from the figure. Although we have preferably taken line-2 which follows well the ridge line we think any lines between line 1 and 3 also might be good candidate for the matching line and we're expecting that if only matching line

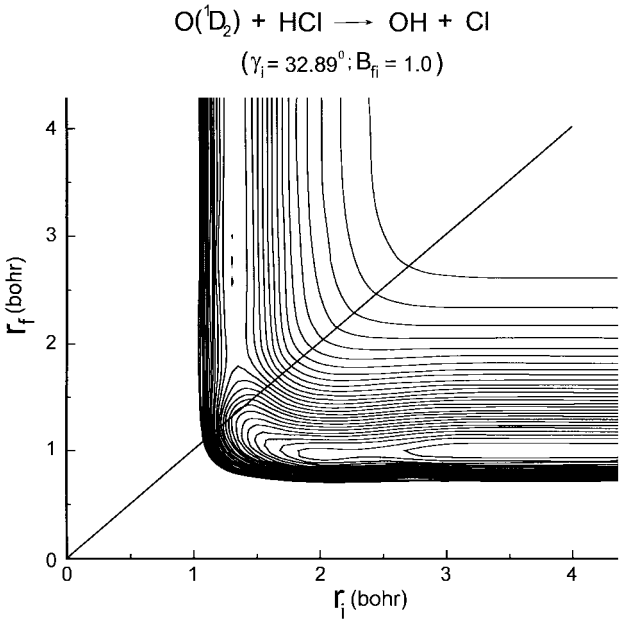

Figure 4. Potential contour of O(¹D) + HCl system as a function of reduce mass Jocobian coordinates- r_i and r_f with γ_i (γ_i = 32.89°) being fixed in the reactant channel, γ_f which is determined by matching coefficient, B_{fi} = 1, being fixed in the product channel. The straight line indicates the matching line.

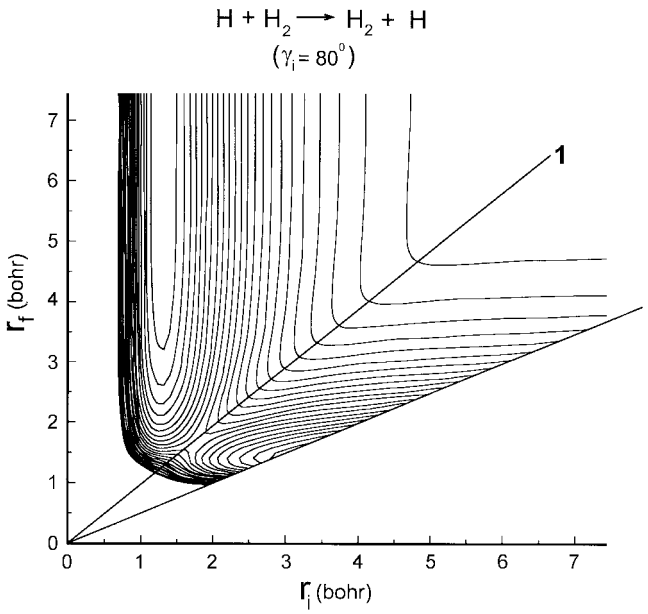

Figure 5. Same as Fig. for H + H_2 system with $\gamma_i = 80°$.

lies in that region the final results will not be much dependent on the value of B_{fi}.

Once the B_{fi} determined, then γ_f is also determined by eq. (7) and we can also make contour figure for fixed γ_f as a function of r_i and r_f. Putting this figure together with the upper part of the matching line - line 2 of Figure 2, it shows the full PES as shown in Figure 4. Figure 4 shows very smooth topography all over the region.

In order to show the effectiveness of the above method for the determination of B_{fi}, we applied this method to the H + H_2 → H_2 + H reaction system in which the B_{fi} is naturally determined to be equal to 1, to see if this method really gives B_{fi} = 1 result. As is shown in Figure 5 (for $\gamma_i = 80°$), the line-1 which is the best choice for the matching line in this contour figure exactly gives the slope to be 1. If we combine the above method with the iterational method proposed by Nakamura *et al.*,[43] it will be more efficient and reasonable for the determination of matching coefficients.

Results and Discussion

A. γ_i averaged cross section and rate constant. In this section we have given the γ_i averaged cross sections and rate constants calculated by us and these are compared with the Schinke's QC cross sections[14] and experimental rate constants.[5] Although recent QC[17,18] results are available we did not make comparison with them, because the PES we have employed are different from them.

The γ_i averaged total cross sections and corresponding QC results[14] are compared in Figure 6. The γ_i averaged state-to-state cross sections are also given in Figure 7. As shown in Figure 6, our results underestimate the cross sections compared with the QC cross sections. Our results are smaller about by 3 or 4 times than the QC counterpart at larger energies, and are too small (about one order) than the QC

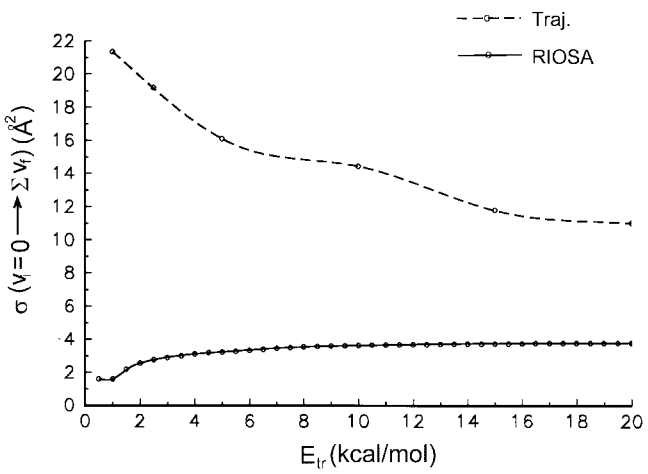

Figure 6. The total reaction cross sections as a function of collision energy for $O(^1D)$ + HCl(v_i = 0) → OH + Cl. Solid line is current RIOSA and dotted line is the QCT from Ref. 14.

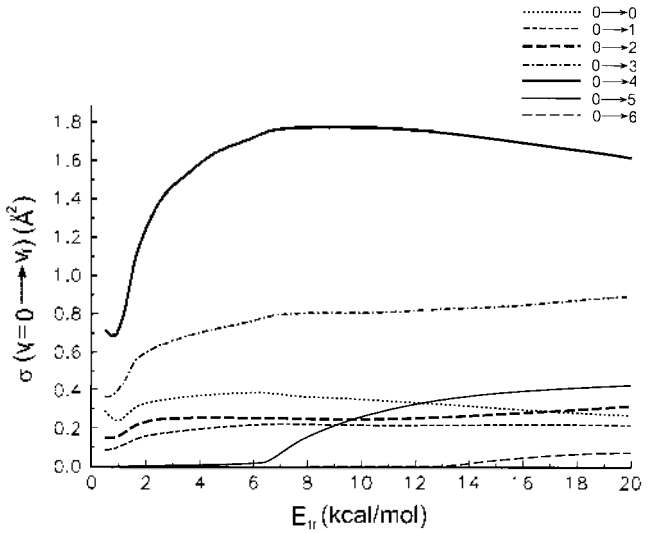

Figure 7. The vibrational state to state reaction cross sections as a function of collision energy for $O(^1D)$ + HCl(v_i = 0) → OH(v_f = 0-6) + Cl calculated using RIOSA.

results at low energies. The larger differences in cross section value at low energies is probably because of the less accuracy of RIOSA at low energy.

It may be more meaningful to observe the shape of the curve of cross sections as a function of energy rather than their absolute value. Our result shows that the cross sections increase at the low energy region and then become nearly independent of the energy at larger energy region, while in QC results that the cross sections are monotonically decreasing at lower energy region and also become nearly independent of energy at larger energy region. These behaviours indicate that the RIOSA is giving reasonable results at least for higher energies.

The state-to-state cross sections show similar behaviour as that of total cross sections. The 0 → 4 and 0 → 3 transitions are dominant over whole region of energy, the 0 → 5

transition increases quickly after its threshold energy and become thirdly dominant transition. The $0 \rightarrow 4$ cross section shows slightly decreasing behaviour at larger energy, in good agreement (at high energy region) with recent cross section measurement.[12] Although deep well persists in current reaction system. both total and state-to-state cross sections show no clear resonance feature.

Using these cross sections rate constants are also calculated in broad range of temperature. Table 1. has compared the calculated rate constants and the experimental rate constants.[5] Because the original experimental rate constants given in Ref. 5 are for the total deactivation of $O(^1D)$, these are multiplied by the branching ratio. 0.67 (67%)[3] in order to obtain the rate constants for the channel (1a). The calculated rates are smaller by 6-10 times than the experimental one. In order to compare these two rates in the same scale the calculated rates are multiplied by 6.7 and also given in the Table. The semilog plot for both experimental and calculated rates (scaled) are depicted in Figure 8. the lines in the figure are made by linear curve fitting.

Their temperature dependence are in fairly good agreement. although noticeable discrepancy exist *i.e.* the line for the calculated one is slightly sloped while the line for the experimental one is nearly not sloped. This indicates that the RIOSA calculation predicts some small but not negligible activation energy while the experiment predicts negligible activation energy. We think this discrepancy might possibly results both from the shortcomings of the PES we have employed and from the shortcomings of the approximation theory we have applied.

Table 1. Rate constants (10^{-10} $cm^3molecule^{-1}sec^{-1}$)

T (K)	k (this work)[a]	$6.7 \times k$ (this work)	k (exp)[b]
199	0.094	0.63	0.94
213	0.10	0.67	1.0
223	0.11	0.74	1.0
230	0.11	0.74	0.87
233	0.11	0.74	0.94
250	0.12	0.80	--
253	0.12	0.80	0.94
262	0.12	0.80	0.87
273	0.13	0.87	0.94
291	0.14	0.94	1.0
292	0.14	0.94	0.94
293	0.14	0.94	0.94
298	0.14	0.94	--
300	0.14	0.94	0.94
314	0.15	1.0	0.94
328	0.15	1.0	1.0
337	0.16	1.1	0.94
354	0.16	1.1	0.94
355	0.16	1.1	0.94
379	0.17	1.1	1.0

[a] Initial vibrational state specified ($v_i = 0$), final state summed rates. [b] Obtained by multiplying 0.67 (Ref. 5) in order to get the rates for the reaction channel (1a).

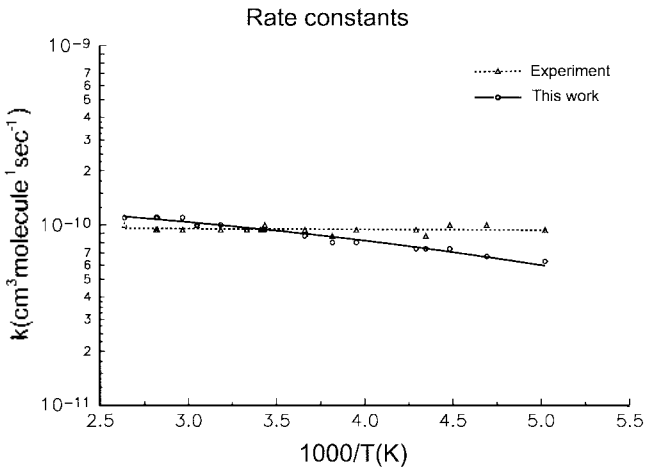

Figure 8. Semilog plot of reaction rate constants as a function of 1000/T for the reaction. Experimental results[4] and scaled RIOSA.

It is encouraging that our results give the same order of cross sections and similar behaviour of energy dependence of cross sections at high energy and also in fairly good agreement of temperature dependence of rate constants with the experiment, in spite of the fact that we have taken considerable approximations. These points partially support the success of RIOSA for the description of current reaction system, it will be very worthwhile to perform furtherly the accurate partial wave summation calculation within the RIOSA. These works are currently under process.

B. γ_i dependent state-to-state $J = 0$ reaction probability and cross sections. In this section we provide the more detailed quantities. the γ_i dependent $J = 0$ state-to-state reaction probability and cross sections. This will help us get more insight into the reaction mechanism. γ_i dependent reaction probability is given by eq. (3), and γ_i dependent cross section is given by[56]

$$\sigma(j_i, v_i \rightarrow v_f, E_{tr}, \gamma_i) = \frac{\pi}{2k^2_{v_i j_i}} \sum_{J_i} (2J_i + 1) P_{J_i}(j_i, v_i \rightarrow v_f, \gamma_i, E_{tr}) \quad (19a)$$

if applying shifting approximation

$$\sigma(j_i, v_i \rightarrow v_f, E_{tr}, \gamma_i) = \frac{\pi}{2k^2_{v_i j_i} B^{\dagger}(\gamma_i)} \int_0^{E_{tr}} d\varepsilon P_{J_i = 0}(j_i, v_i \rightarrow v_f, \gamma_i, \varepsilon) \quad (19b)$$

We presented the results for three chosen γ_i angles. γ_i = 9.27°, 32.89° and 64.81°. as shown in Figure 9a(b), Figure 10a(b), Figure 11a(b). They show quite different behaviours for each different γ_i. indicating strong steric effect which will be discussed in the next section in detail. The energy dependence of reaction probabilities are more and more structured with the increase of γ_i. while the cross sections are always smoothly changing with the change of energy.

At near collinear approach. γ_i = 9.27°. reaction probability is rapidly increasing with the energy from very small value

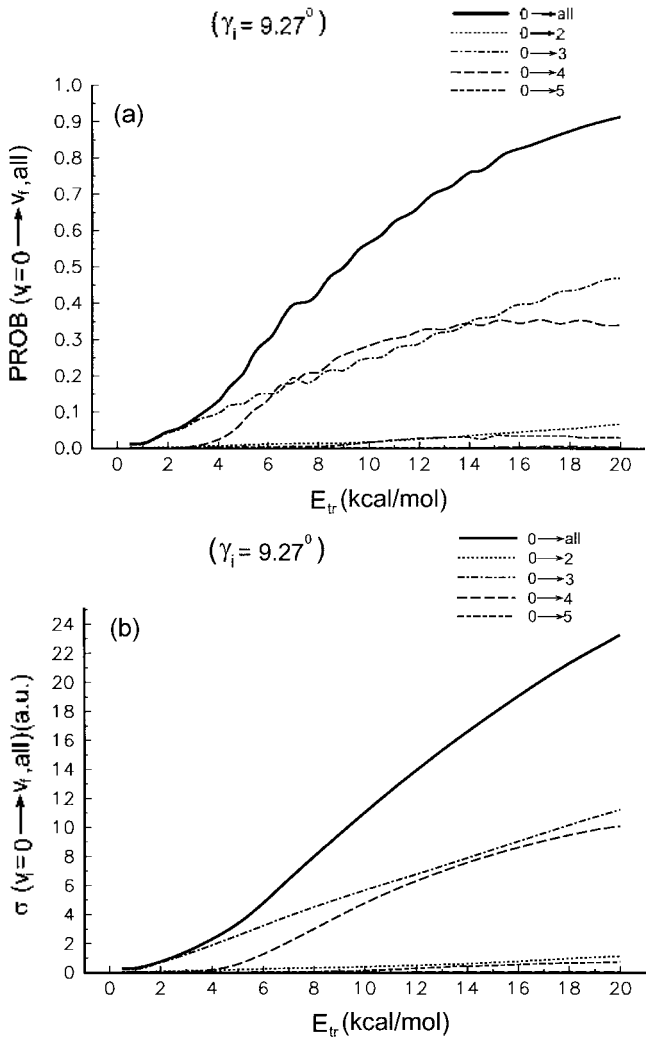

Figure 9. (a) The angle dependent vibrational state to state and total reaction probabilities as a function of collision energy at γ_i = 9.27° with l_i = 0. (b) The angle dependent vibrational state to state and total reaction cross sections as a function of collision energy at γ_i = 9.27° with the shifting approximation.

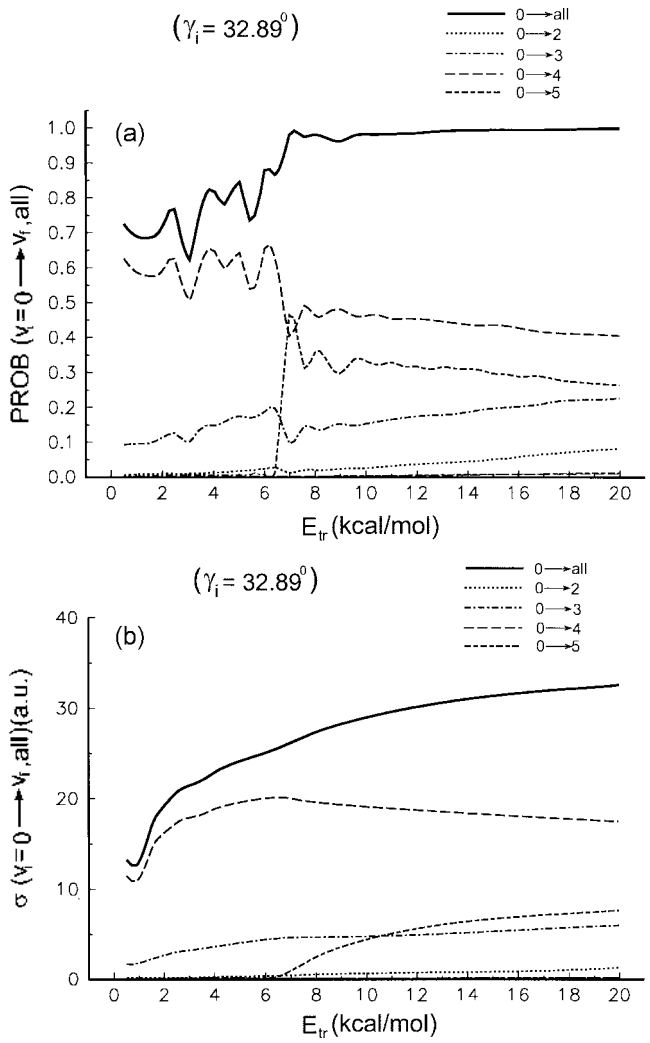

Figure 10. (a) Same as Figure 9a. at γ_i = 32.89° with l_i = 0. (b) Same as Figure 9b. at γ_i = 32.89° with the shifting approximation.

of probability at low energy, and also seem to show regular oscillations with negligibly small amplitude. At the larger angle, γ_i =32.89°, the reaction probability is very large at low energy and increases with the energy accompanying strong oscillation. They increase and oscillate until the magnitude of the reaction probability nearly equal to 1, since then, the oscillation disappears and reaction probability no more changes preserving quite high value of probability ($\approx$ 1). At γ_i = 64.81°, the oscillation is much stronger than the other two angles with nearly constant (slightly decreasing) and high value of average reaction probability ($\approx$ 0.9).

These different behaviors of the magnitude of reaction probability and the extent of oscillation along with the energy for different γ_i are probably mainly due to the PES topography. The kinematics also might contribute to the oscillatory behaviors. the oscillatory behavior of the collinear Heavy-Light-Heavy system is well known, and in fact the evident regular oscillation is found for the collinear arrangement of current reaction system although we have not presented here. However we think in case of non-collinear arrangements ($\gamma_i \neq 0$) kinematics play only minor role in current reaction system. this can be derived from the negligibly small oscillatory behavior for the near collinear arrangement, γ_i = 9.27°, it seems to indicate that the kinematic effect almost disappears if only the system deviates slightly from the collinear arrangement.

The PES we employed has the largest barrier at the collinear arrangement and this barrier is lowering with the increase of γ_i[14] Among the three angles we have chosen, γ_i =9.27° configuration has the largest barrier and much lowered barrier at γ_i = 32.89° while no barrier exists for the γ_i = 64.81° configuration. these features are probably responsible for the rapid increase, slow increase, nearly constant (slightly decreasing) average reaction probability with the energy for each γ_i. The oscillatory feature is probably due to the resonances, and this feature is closely related to the PES topography. At near collinear configuration, the VAP is quite repulsive and no potential well exists in the VAP curves, and at larger γ_i there begin to appear the potential well in the

VAP curves and the larger the γ_i the deeper the well. This is because of the bent configuration structure of the deep potential well[14] of the reaction system. Larger γ_i approach will allow passing through the deeper part of the potential well. At larger γ_i, almost all the VAP curves corresponding to each vibrational channels possess deep wells. These wells could support large number of bound and quasi-bound states in the interaction region and this inevitably leads to the strong resonance feature for the reaction probability. Further detailed analyses such as Argand diagram method is needed to confirm whether these oscillations are really due to the resonances or just the ordinary feature of the Heavy-Light-Heavy reaction systems.

In spite of the strong oscillatory feature in the reaction probability for larger γ_i, the cross section is showing quite smooth behaviour. This is because oscillation is averaged out in the calculation of the cross section. Although in this work we employed shifting approximation for the calculation of the cross sections we think that even in the more accurate partial wave summation calculation the cross sections may not necessarily show significant peaks. because reaction probability is oscillating quite regularly with short period, and different partial wave probabilities will be peaked at shifted position. so the peaks and dips could cancel out each other. Moreover because of the heavy reduced mass, this shifting is expected to be quite small, (from the point of view of shifting approximation) this lets the 'cancel out' be working in a continuous way.

The small peak near 3.5 kcal/mol found in Figure 11b is due to the irregular oscillation of the reaction probability in that energy region as shown in Figure 11a, *i.e.* the sharp peak of the reaction probability at this energy is followed by a exceptionally large dip at about 4.5 kcal/mol as shown in Figure 11a. In order to understand the dip nature in Figure 11a and the smoothness of the cross sections in Figure 11b, more accurate quantum mechanical calculation with accurate PES should be required.

C. Steric effects. Steric effect is described by the steric factor which is defined by the γ_i dependent total cross section given by[57]

$$\sigma(j_i,v_i;E_{tr},\gamma_i) = \sum_{v_f} \sigma(j_i,v_i \rightarrow v_f;E_{tr},\gamma_i) \qquad (20)$$

where $\sigma(j_i,v_i \rightarrow v_f;E_{tr},\gamma_i)$ is the γ_i dependent state-to-state cross section given by eq. (19).

The steric factors for several chosen energies are shown together in Figure 12. These figures show strong steric effect. Two significant broad peaks are the most conspicuous. and a small peak is also found near 90°. Very similar steric factor curves are found for $He + H_2^+$ and $Ar + H_2^-$ systems by Baer and Nakamura.[38] The PES of the two systems are nearly independent to the γ_i angles, so Baer and Nakamura explained the quite structured steric factors are mainly due to the kinematic effects. In case of current reaction system. the feature of steric factors are determined both by kinematics and PES. The small value at small angles are due to the relatively larger barrier. and the minimum at about γ_i approx 45° is probably due to the kinematic effect, because at this angle the barrier disappears.

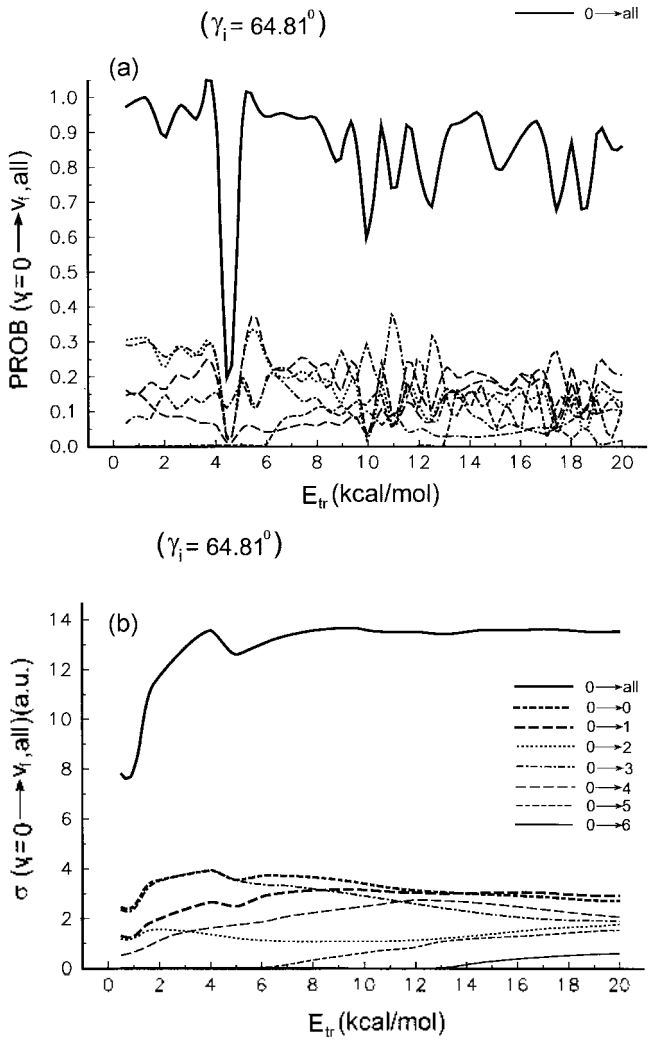

Figure 11. (a) Same as Figure 9a. at $\gamma_i = 64.81°$ with $l_i = 0$. (b) Same as Figure 9b. at $\gamma_i = 64.81°$ with the shifting approximation.

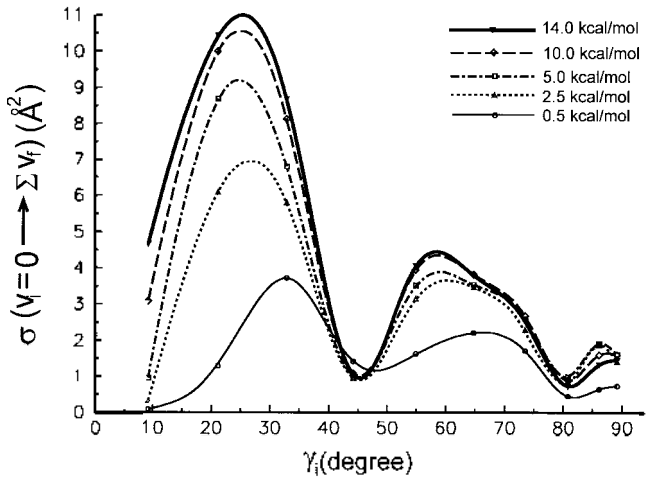

Figure 12. The steric factor curves as a function of γ_i for several chosen collision energies.

At the larger energy, the steric factors are weakly dependent on the energy both in their qualitative and quantitative features. However they show some changes with the energy. These changes are more significant at low energy. The absolute magnitude of the cross sections are showing steady increase and the two broad peaks are slightly shifting to the smaller angles with the increase of the energy, and the cross sections are rapidly increasing at small angles (near collinear) with the energy. This feature implies that abstraction type of reaction will take more and more important role in the reaction dynamics while energy is increasing.

Generally, the reaction mechanisms are divided into two types. One is the abstraction type, in which the reaction occurs directly without formation of the intermediate complexes, and another one is the insertion type, in which the reaction occurs less directly with the formation of some lifetime of intermediate complexes during the reaction. These two types of mechanisms lead to different dynamical appearances. However there is no rigorous definition for this two types of reaction mechanisms. In the current RIOSA study, we may define the types of the reaction according to the angles γ_i the reaction approached. As already mentioned, the larger angle will allow the reaction system to pass through the deeper part of the potential well, so it favors the formation of longer lifetime of complexes. Therefore for the larger angle approaches the reaction will occur more indirectly, so it may be grouped into the insertion type of reaction, and for the smaller angle approaches the reaction will occur more directly, it may be grouped into the abstraction type of reaction.

However it's ambiguous where to define the boundary angle at which the two different types of reactions are separated. In this paper, instead of defining the boundary angle at which the abstraction type and insertion type of reaction are strictly separated, we would rather define an angle from the point of view of vibrational distribution as discussed in the following section. We define such an angle so that the γ_i dependent vibrational distributions are showing two noticeably different types of features in each region of the angles separated by the boundary angle, and within each region the γ_i dependent vibrational distributions will not be much dependent on the γ_i.

We think this angle could be roughly chosen at $\gamma_i \simeq 40°$ which lies between the two broad peaks in the steric factor curves. Such choice is making sense if we consider the vibrational distributions at both sides of this angle. As will be shown in the next section, the vibrational distributions show quite different features at both sides of this angle, while within each side the vibrational distributions are not changing significantly with the angles. At the angles less than $\gamma_i \simeq 40°$, the vibrational distributions show highly excited vibrational distribution, only $v_f = 3, 4$ states are significantly populated with no population on the other vibrational states. And at the angles larger than γ_i simeq 40°, the vibrational distributions begin to show much relaxed distribution *i.e.* significant distributions appear for low vibrational states, $v_f = 0, 1, 2$ and consequently show the bimodal distributions.

These two quite different features of vibrational distributions in each region divided by the boundary angle indicate the reaction undergoes through different type of mechanisms. We think the reactions with the angles smaller than the boundary angle are occurring more directly and the reactions with the angles larger than the boundary angle are occurring more indirectly. Thus we considered the reaction mechanisms in terms of 'direct' and 'indirect' instead of 'abstraction' and 'insertion'. Although the abstraction type of reactions always take place directly, the insertion type of reactions might take place either indirectly or directly depending upon whether the lifetimes of the intermediate complexes formed during the reaction are long enough to allow the energy to be fully equipartitioned or not before breaking into the product pieces.

From the both features, the relations of vibrational distribution with the angle and the two broad peaks in the steric factor curves, we can conclude both types of reaction mechanisms (direct and indirect) are equally important in current reaction system.

D. Vibrational distribution. As shown in the previous section, strong steric effects are present in current reaction system. These steric effects are also reflected in the γ_i dependent vibrational distributions. The two broad large peaks shown in the steric factor curves are very important for the overall feature of the vibrational distribution, because the largest contribution to the cross sections mainly comes from this two peaks. Therefore we have sampled one angle (32.89°) at the first peak, and two angles (64.81° and 73.54°) at the second peak to discuss the γ_i dependent vibrational distributions. Another small angle (9.27°) is also chosen although this angle has only small contribution to the cross section, to see the vibrational distribution for quasicollinear approach in this case the reaction probably occurs *via* abstraction.

Although the γ_i dependent vibrational distributions are

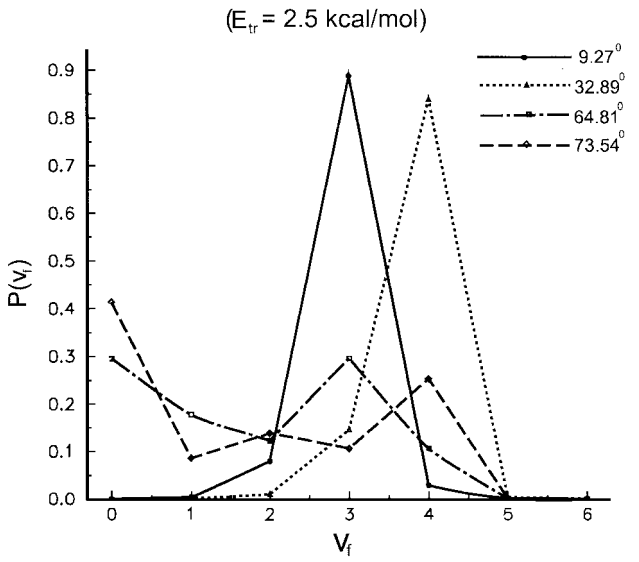

Figure 13. Angle dependent vibrational distribution for several chosen γ_i angles, at collision energy 2.5 kcal/mol.

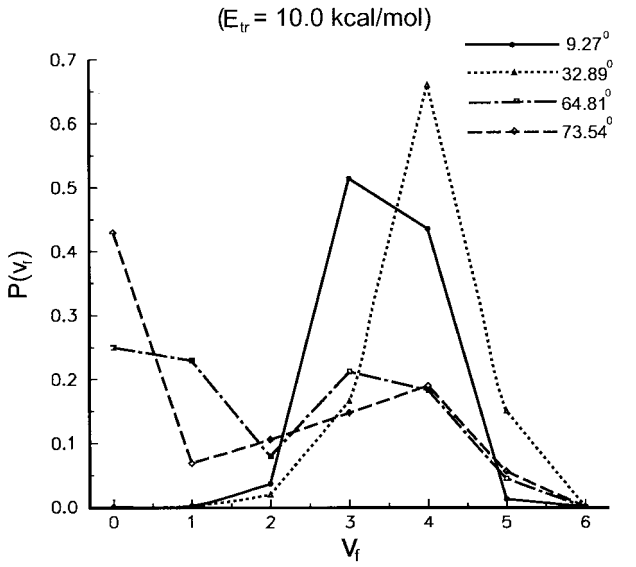

Figure 14. Same as Figure 13. at collision energy 10.0 kcal/mol.

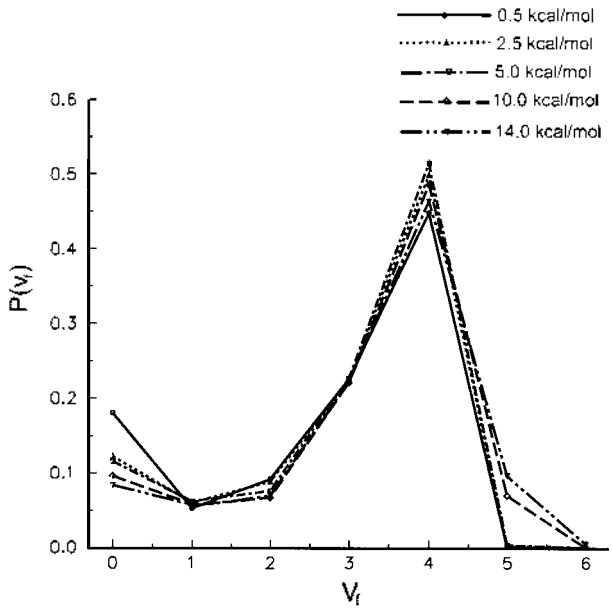

Figure 15. Vibrational distribution for several chosen collision energies. These results are compared with QCT[14] and Experimental results.[2,11]

provided only for the four angles. the distributions for the other angles are very similar to one of these four angles we have chosen. For those angles at the first peak. the distributions are very similar to that of γ_i = 32.89°. and for those angles at the second peak the distributions are very similar to that of γ_i = 64.81° or 73.54°.

The γ_i dependent vibrational distributions for four chosen angles (γ_i = 9.27°, 32.89°, 64.81°, and 73.54°) are given in Figure 13 for E_{tr} = 2.5 kcal/mol, and Figure 14 for E_{tr} = 10.0 kcal/mol. γ_i averaged overall vibrational distributions are also shown in Figure 15 for several chosen energies. Those distributions are defined in terms of relative cross sections.

The vibrational distributions show quite different features with the γ_i. The most noticeable difference is between the distributions for smaller angles (9.27°. 32.89°) and the distributions for larger angles (64.81°, 73.54°). At smaller angles the highly excited unimodal distribution is found. the most population is concentrated on v_f = 3, 4 states (v_f = 5 state also for higher energies). On the other hand. bimodal distribution is found for the larger angles, in this case v_f = 0 state is always highly populated and the highly excited states (v_f = 3. 4) are also showing considerable populations.

These γ_i dependent vibrational distributions indicate that for the smaller angles corresponding to the first peak in the steric factor curve. the reaction is dominated by the direct reaction mechanism. and for the larger angles corresponding to the second broad peak in the steric factor curve, both direct and indirect reaction mechanisms are equally important. These features are related to the potential energy topography. The larger the angle approached the deeper part of the potential well is passed through and consequently the longer lifetime of complex is allowed.

It seems that although the potential wells begin to appear in the VAP curve for the smaller angles at the fist peak of the steric factor curve, the well is not deep enough to support long enough lifetime for the relaxation of highly excited vibrational states. Even for the larger angles which possess deep or the deepest potential well. the vibrational distributions are not fully relaxed. they are showing also significant populations in the high vibrational states. This indicates that even in case of the reaction system passes through the deepest potential well the complex is broken into the products before the energy is fully equipartitioned.

These features imply that the direct reaction mechanism is always playing an important role whether the reaction passes through deep or shallow part of the potential well. γ_i averaged overall vibrational distributions shown in Figure 15 is the result of two competing contributions from two broad peaks in the steric factor curve. It shows the maximum population at v_f = 4 and v_f =3, 4 are dominantly populated. This feature is in quite good agreement with recent two experiments.[2,11] Figure 15 also shows small peak at v_f =0, consequently the overall vibrational distributions are showing the bimodal feature, and such a feature is never detected in the previous experimental or theoretical studies. We are not able to confirm whether the peak appearing at v_f = 0 state really exists in current reaction system or whether it is artifact of the PES. In fact. the QC study[14] also found considerable population at v_f = 0 state. Surprisingly our result for the population at this state is in quantitative agreement with that of QC result.[14] The vibrational distribution obtained in QC study is in fairly good agreement with our quantum results. The QC study found broad population over the v_f = 0-5 states. but it does not show bimodal feature, and the populations are evenly distributed over v_f = 0-4 states while our quantum result shows sharp distribution *i.e.* exceptionally large population for v_f = 4 state.

The bimodal feature in γ_i averaged overall vibrational distributions and the relative magnitude between the population

at low state (v_f = 0) and high states indicate that while both the direct and indirect reaction mechanisms are playing important role, the direct mechanism is dominant over the indirect mechanism. This does not mean that the abstraction type of reaction dominates over the insertion type of reaction, because as mentioned in the previous section insertion type of reaction may occur directly.

These figures also show that vibrational distributions are weakly dependent on the energy both qualitatively and quantitatively, especially in case of γ_t averaged distributions. In case of γ_t averaged distribution, although the distribution is slightly changing with the energy some interesting feature is worthy to be noted. Each vibrational states behave differently with the energy. When the energy is increasing the populations for v_f = 1, 2, 3 states are almost not changing at all, while the populations for the other states -v_f = 0, 4, 5 are showing small but noticeable changes. The population for v_f = 4 is first increasing with the energy until about 5.0 kcal/mol and then decreasing with the energy. On the other hand v_f = 0, 5 states are showing monotonic change *i.e.* with the increase of energy v_f = 0 state is monotonically decreasing and v_f = 5 state is monotonically increasing. These features indicate that with the increase of energy direct reaction mechanism is becoming more and more dominant.

Acknowledgment. This article is dedicated to professor Kyung-Hoon Jung at KAIST on the occasion of his 65 anniversary. This work was supported in part by the KOSEF. R01-1999-00035 and the BK21 project from the Ministry of Education of Korea. S.C.P is grateful to the Korea Institute of Science and Information Technology (KISTI) for allowing us to access the CRAY-C90.

References

1. Cicerone, R. J. *Science* **1987**, *237*, 35.
2. Kruus, E. J.; Niefer, B. I.; Sloan, J. J. *J. Chem. Phys.* **1988**, *88*, 985.
3. Wine, P. H.; Wells, J. R.; Ravishankara, A. R. *J. Chem. Phys.* **1986**, *84*, 1349.
4. Davidson, J. A.; Sadowski, C. M.; Schiff, H. I.; Streit, G. E.; Howard, C. J.; Jennings, D. A.; Schmeltekopf, A. L. *J. Chem. Phys.* **1976**, *64*, 57.
5. Davidson, J. A.; Schiff, H. I.; Streit, G. E.; McAfee, J. R.; Schemltekopf, A. L.; Howard, C. J. *J. Chem. Phys.* **1977**, *67*, 5021.
6. Addison, M. C.; Donovan, J. R.; Gillespie, H. M. *Chem. Phys. Lett.* **1976**, *44*, 602.
7. Basco, N.; Norrish, R. G. W. *Proc. R. Soc. London Ser.* **1961**, *A 260*, 293.
8. Balucani, N.; Beneventi, L.; Casavecchia, P.; Volpi, G. G. *Chem. Phys. Lett.* **1991**, *180*, 34.
9. Matsumi, Y.; Tonokura, K.; Kawasaki, M.; Tsuji, K.; Obi, K. *J. Chem. Phys.* **1993**, *98*, 8330.
10. Luntz, A. C. *J. Chem. Phys.* **1980**, *73*, 5393.
11. Park, C. R.; Wiesenfeld, J. R. *Chem. Phys. Lett.* **1989**, *163*, 230.
12. Alexander, A. J.; Brouard, M.; Rayner, S. P.; Simons, J. P. *Chem. Phys.* **1996**, *207*, 215.
13. Alexander, A. J.; Brouard, M.; Rayner, S. P.; Simons, J. P. *1995 Conference on the Dynamics of Molecular Collisions*; Asilomar, California, July 16-21, 1995; p PB51.
14. Schinke, R. *J. Chem. Phys.* **1984**, *80*, 5510.
15. Liu, B. (unpublished).
16. Rynefors, K.; Elofson, P. A.; Holmlid, L. *Chem. Phys.* **1985**, *100*, 53.
17. Laganà, L.; Ochoa de Aspuru, G.; Garcia, E. *J. Phys. Chem.* **1995**, *99*, 17139.
18. Luz Hernandez, M.; Redondo, C.; Laganà, L.; Ochoa de Aspuru, G.; Rosi, M.; Sgamellotti, A. J. *Chem. Phys.* **1996**, *105*, 2710.
19. Mirri, A. M.; Scappini, F.; Cazzoli, G. J. *Mol. Spectrosc.* **1971**, *38*, 218.
20. Bruna, P. J.; Hirsch, G.; Peyerimhoff, S. D.; Buenker, R. J. *Can. J. Chem.* **1979**, *57*, 1839.
21. Hirsch, G.; Bruna, P. J.; Peyerimhoff, S. D.; Buenker, R. J. *Chem. Phys. Lett.* **1977**, *52*, 442.
22. Turner, A. G. *Inorg. Chem. Acta* **1986**, *111*, 157.
23. Huber, K. P.; Herzberg, G. *Constants of Diatomic Molecules*; Van Nostrand: New York, 1978.
24. Badenhoop, J. K.; Koizumi, K.; Schatz, G. C. *J. Chem. Phys.* **1989**, *91*, 142.
25. Khare, V.; Kouri, D. J.; Baer, M. *J. Chem. Phys.* **1979**, *71*, 1188.
26. Barg, G. D.; Drolshagen, G. *Chem. Phys.* **1980**, *47*, 209.
27. Bowman, J. M.; Lee, K. T. *J. Chem. Phys.* **1978**, *68*, 3940.
28. Bowman, J. M.; Lee, K. T. *Chem. Phys. Lett.* **1979**, *64*, 291.
29. Bowman, J. M.; Lee, K. T. *J. Chem. Phys.* **1980**, *72*, 5071; **1980**, *73*, 3522(E).
30. Baer, M.; Khare, V.; Kouri, D. J. *Chem. Phys. Lett.* **1979**, *68*, 378.
31. Baer, M.; Mayne, H. R.; Khare, V.; Kouri, D. J. *Chem. Phys. Lett.* **1980**, *72*, 269.
32. Kouri, D. J.; Khare, V.; Baer, M. J. *Chem. Phys.* **1981**, *75*, 1179.
33. Baer, M. *Adv. Chem. Phys.* **1982**, *49*, 191.
34. Khare, V.; Kouri, D. J.; Jellinek, J.; Baer, M. In *Potential Energy Surfaces and Dynamics Calculations*; Truhlar, D. G., Ed.; Plenum: New York, 1981; pp 475-493.
35. Jellinek, J.; Kouri, D. J. In *Theory of Chemical Reaction Dynamics*; Baer, M., Ed.; Chemical Rubber: Boca Raton, FL, 1985; Vol II, Ch. 1.
36. Baer, M.; Kouri, D. J. In *The Theory of Chemical Reaction Dynamics*; Clary, D. C., Ed.; Reidel, Dordrecht: 1986; p 167.
37. Jellinek, J.; Baer, M. *J. Chem. Phys.* **1983**, *78*, 4494.
38. Baer, M.; Nakamura, H. *J. Phys. Chem.* **1987**, *91*, 5503.
39. Jellinek, J.; Kouri, D. J. *J. Chem. Phys.* **1984**, *80*, 3114.
40. Baer, M.; Kouri, D. J.; Jellinek, J. J. *Chem. Phys.* **1984**, *80*, 1431.
41. Jellinek, J. *Chem. Phys. Lett.* **1985**, *114*, 210.
42. Jellinek, J. J. *Math. Phys.* **1985**, *26*, 1397.
43. Nakamura, H.; Ohsaki, A.; Baer, M. *J. Phys. Chem.* **1986**, *90*, 6176.
44. Ohsaki, A.; Nakamura, H. *Phys. Rep.* **1990**, *187*, 1.
45. Bowman, J. M. *Adv. Chem. Phys.* **1985**, *61*, 115.
46. Bowman, J. M. *J. Phys. Chem.* **1991**, *95*, 4960.
47. Park, S. C.; Nakamura, H.; Ohsaki, A. *J. Chem. Phys.* **1990**, *92*, 6538.
48. Steinfeld, J. I.; Francisco, J. S.; Hase, W. L. *Chemical Kinetics and Dynamics*; Prentice-Hall, Inc.: 1989.
49. Wigner, E. P.; Eisenbud, L. *Phys. Rev.* **1947**, *72*, 29.
50. Lane, A. M.; Thomas, R. G. *Rev. Mod. Phys.* **1958**, *30*, 257.
51. Zvijac, D. J.; Light, J. C. *Chem. Phys.* **1976**, *12*, 237.
52. Light, J. C.; Walker, R. B. *J. Chem. Phys.* **1976**, *65*, 4272.
53. Light, J. C. In *The Theory of Chemical Reaction Dynamics*; Clary, D. C., Ed.; Reidel, Dordrecht: 1986; p 215.
54. Kuppermann, A. *Chem. Phys. Lett.* **1975**, *32*, 374.
55. Kuppermann, A. In *Advances in Molecular Vibrations and Collision Dynamics*; Bowman, J. M., Ed.; JAI: Greenwich, 1994; Vol. 2B, p 117 and references there in.
56. It is more appropriate to define the γ_t dependent cross section as

$$\sigma(j_i, v_i \rightarrow v_f, E_{tr}, \gamma_t) = \frac{\pi}{k^2_{v_i j_i}} \sum_{l_i} (2l_i - 1) P_{l_i}(j_i, v_i \rightarrow v_f, \gamma_t, E_{tr})$$

because $\frac{1}{2}\int_0^{\pi} \sin\gamma_t d\gamma_t = 1$ our definition is different from this definition by a factor 0.5. The reason we used eq. (19) is that our program gave the γ_t dependent cross section datas in a form of it.
57. Note: This definition is different from the definition in Ref. 38 by a factor 0.5.